Artificial Intelligence in Agriculture 1 (2019) 1–8

Contents lists available at ScienceDirect

Artificial Intelligence in Agriculture

journal homepage: http://www.keaipublishing.com/en/journals/artificial-intelligence-in-agriculture/

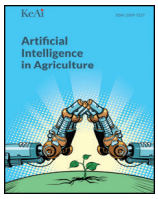

Fusion of machine vision technology and AlexNet-CNNs deep learning network for the detection of postharvest apple pesticide residues

Bo Jiang [a,b,c], Jinrong He [b,c,d], Shuqin Yang [a,b,c], Hongfei Fu [e], Tong Li [a,b,c], Huaibo Song [a,b,c,*], Dongjian He [a,b,c]

[a] College of Mechanical and Electronic Engineering, Northwest A&F University, Yangling, Shaanxi 712100, China
[b] Key Laboratory of Agricultural Internet of Things, Ministry of Agriculture and Rural Affairs, Yangling, Shaanxi 712100, China
[c] Key Laboratory of Agricultural Information Perception and Intelligent Services, Yangling, Shaanxi 712100, China
[d] College of Information Engineering, Northwest A&F University, Yangling, Shaanxi 712100, China
[e] College of Food Science and Engineering, Northwest A&F University, Yangling, Shaanxi 712100, China

ARTICLE INFO

Article history:
Received 16 November 2018
Received in revised form 27 January 2019
Accepted 4 February 2019
Available online 14 March 2019

Keywords:
Pesticide residue detection
Apple
Hyperspectral
CNN network
KNN
SVM

ABSTRACT

Pesticide residue is an important factor that affects food safety. In order to achieve effective detection of pesticide residues in apples, a machine-vision-based segmentation algorithm and hyperspectral techniques were used to segment the foreground and background regions of the apple image. By calculating the roundness value and extracting the region with the highest roundness value in the connected region, a region of interest (ROI) mask was created for the apple. Four pesticides (chlorpyrifos, carbendazim and two mixed pesticides) and an inactive control were used at the same concentration of 100 ppm (except for the control group), and the hyperspectral region of the corresponding sample image was extracted by obtaining the different types of pesticide residues in the ROI masks. To increase the diversity of the samples and to expand the dataset, Gaussian white noise with a varying signal-to-noise ratio was added to each of the hyperspectral images of the apple. The number of samples was increased from four types of 12 samples to four types of 72 samples, giving 4608 hyperspectral data images in each category. The structure and parameters of a convolutional neural network (CNN) were determined using theoretical analysis and experimental verification. All the extracted hyperspectral images of apples were normalized to 227 × 227 × 3 pixels as the input of the CNN network for pesticide residue detection. There were 18,432 sample data of four types for 72 samples. Of these, 12,288 images were selected using a bootstrap sampling method as the training set, and 6144 as the test set, with no overlap. The test results show that when the number of training epochs was 10, the accuracy of the test set detection was 99.09%, and the detection accuracy of the single-band average image was 95.35%. A comparison with traditional k-nearest neighbor (KNN) and support vector machine classification algorithms showed that the detection accuracy for KNN was 43.75% and the average time was 0.7645 s. These results demonstrate that our method is a small-sample, non-contact, fast, effective and low-cost technique that can provide effective pesticide residue detection in postharvest apples.

1. Introduction

According to Food and Agriculture Organization statistics from 2013, the production of apples ranks second in the world (Czernyszewicz, 2016). Although pesticides can increase the yield of apples, they also increase the risk to the safety of food (Jiyun et al., 2014). Pesticide residues in apples are one of the most important factors affecting their safety (Liang and Xie, 2017; Jia et al., 2017). A great deal of attention has been paid to the problem of pesticide residues in apples, and effective pesticide residue detection methods are important in restricting production by fruit farmers and improving the level of information for pesticide detection.

In prior research into fruit and vegetable pesticide residue detection, researchers have carried out numerous studies and have proposed a variety of effective detection methods. In view of the different components and types of pesticide residue in apples, Zhou (Wei, 2017) proposed a method for the detection of pesticide residues in apple juice involving cloud point extraction, gas chromatography and mass spectrometry that can achieve the separation of 45 organophosphorus pesticides. This method can accurately detect information about pesticide residue in apples and categorize it. However, this method suffers from lossy detection, and the operation is so complex that it is not suitable for the large-scale detection of pesticide residues in apples. Lei (Peng et al., 2014) proposed the use of multi-spectral fluorescence

* Corresponding author at: College of Mechanical and Electronic Engineering, Northwest A&F University, Yangling, Shaanxi 712100, China.
E-mail address: songhuaibo@nwsuaf.edu.cn (H. Song).

https://doi.org/10.1016/j.aiia.2019.02.001

image technology to detect pesticide residues, and found that under excitation by ultraviolet light at 190–300 nm, fruit containing organophosphorus pesticides produced significant fluorescence near 440 nm, which can be used to accurately detect the presence or absence of pesticide residues in apples. However, this method requires the experimental parameters to be configured in advance, and the experimental results are not stable. Zhu et al. (2017) put forward a method for detecting pesticide residues in apples by laser. Based on established fluorescence data for various types of pesticide residues, an empirical formula was established for an analysis of whether apples contain pesticide residues, using spectral data analysis. However, this method has a low true positive rate, high time costs and a slow detection speed. Liu (Yande et al., 2017) proposed the detection of Imipenem pesticide residues in navel oranges using surface-enhanced Raman spectroscopy. The correlation coefficient and predicted mean square root for this method were 0.919 and 3.990 mg/L respectively. This method has a high detection accuracy, but the operational cost is also high. Li (Zengfang et al., 2016) proposed a method for detecting pesticide residues on the surface of a Gannan navel orange, based on hyperspectral imaging technology, and for realizing the nondestructive detection of agricultural residues by extracting characteristic bands for principal component analysis. Zhang and Li (2018) proposed a full-convergence neural network for hyperspectral transmission imaging, which was used to segment blueberry bruises and flower buds. Wang et al. (2018) applied high-spectral transmittance data with a deep learning architecture to accurately and quickly detect mechanical damage inside blueberries. Jiang et al. (2016) used NIR hyperspectral imaging technology to detect pesticide residues in mulberry leaves. Hyperspectral characteristic bands in mulberry leaves were extracted, analyzed and processed via continuous projection and stepwise regression. The detection accuracy was high, but the complexity of the algorithm was also significant.

We therefore put forward a small-sample, non-contact, low-cost, fast, efficient and non-destructive method for detecting apple pesticide residues under hyperspectral conditions. By taking the advantage of the numerous sample bands in hyperspectral technology, a method is proposed for the detection of hyperspectral pesticide residues in apples based on machine vision technology and CNNs. Based on a collection of high-spectrum apple pesticide residues, a hyperspectral image of an apple was analyzed to extract a mask image corresponding to the type of pesticide residue. The structure and parameters for a CNN network were designed based on the AlexNet framework using the characteristics of hyperspectral apple images. The extracted hyperspectral images were used to train and test the network performance, and finally to realize the rapid and effective non-destructive detection of pesticide residues in apples.

2. Materials and methods

2.1. Materials

Postharvest samples of Fushi apples were collected from the Yangling Apple Agricultural Demonstration Station in June 2016. A hyperspectral instrument (HyperSIS-VNIR-PFH of Zhuoli Hanguang ZOLIX model) was used, as shown in Fig. 1. Three samples of hyperspectral data for pesticide residue were collected for each of four pesticides, which were sprayed on the apples: chlorpyrifos, mycelium, two mixed pesticides (mixtures of chlorpyrifos and carbendazim) and an inactive control. The spectral wavelength range was 865.11–1711.71 nm, and the spectral resolution was 3.32 nm. There were 12 samples in total, and each individual sample contained 256 bands of hyperspectral data.

The data samples for the four pesticide residues were labeled as A (chlorpyrifos), AB (two mixed pesticides), B (carbendazim), and K (inactive control). Each pesticide residue contained three different samples of data, each of which contained 256 bands of spectral data, giving 768 spectral data images in total for each pesticide residue. In order to increase the diversity of the samples, Gaussian white noise with signal-to-noise ratios of 1, 2, 3, 4 and 5 dB was added to the hyperspectral image of the apple for each pesticide residue. This increased the number of samples from 12 in four categories to 72 in four categories, giving 4608 spectral data images in each category. Using a bootstrap sampling method, the sample set was randomly divided into a training set and test set. The training set sample contained 66.7% of the data, with 48 training samples, that is, 12 samples for each type of pesticide residue sample. The test set sample was 33.3% of the data, with 24 samples, giving a total of 48 training samples, that is, six samples for each kind of pesticide residue sample. There was no overlap between the training and the testing sample sets.

The processor for the subsequent training and test processing platform was a 3.4 GHz Inter Core i5-7200 M with 16 GB memory and 500 GB hard disk, and the development platform for the algorithm was MATLAB 2016b. When the hyperspectral image was obtained, the

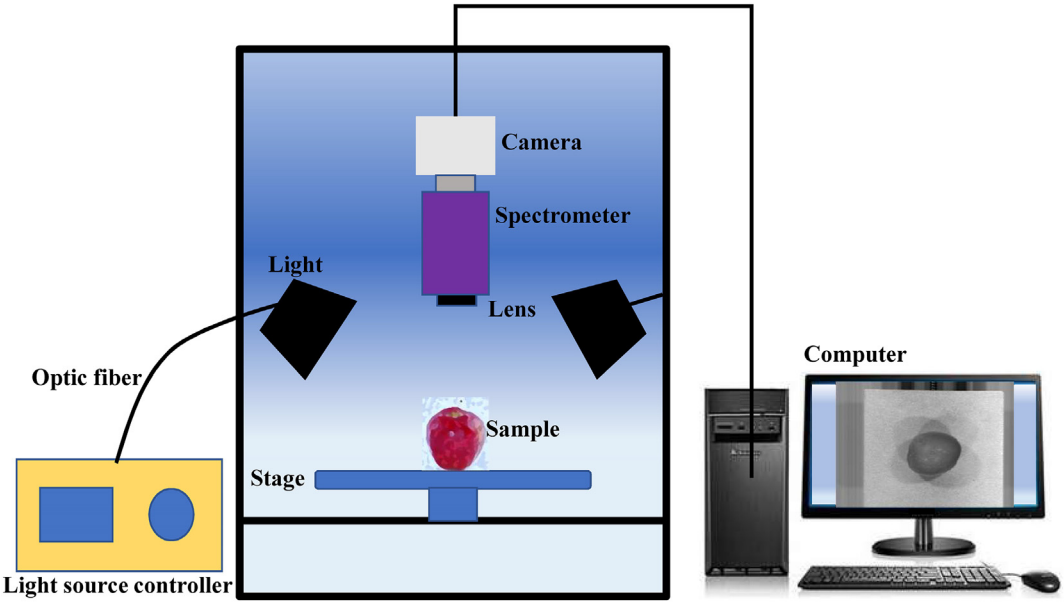

Fig. 1. Hyperspectral imaging system.

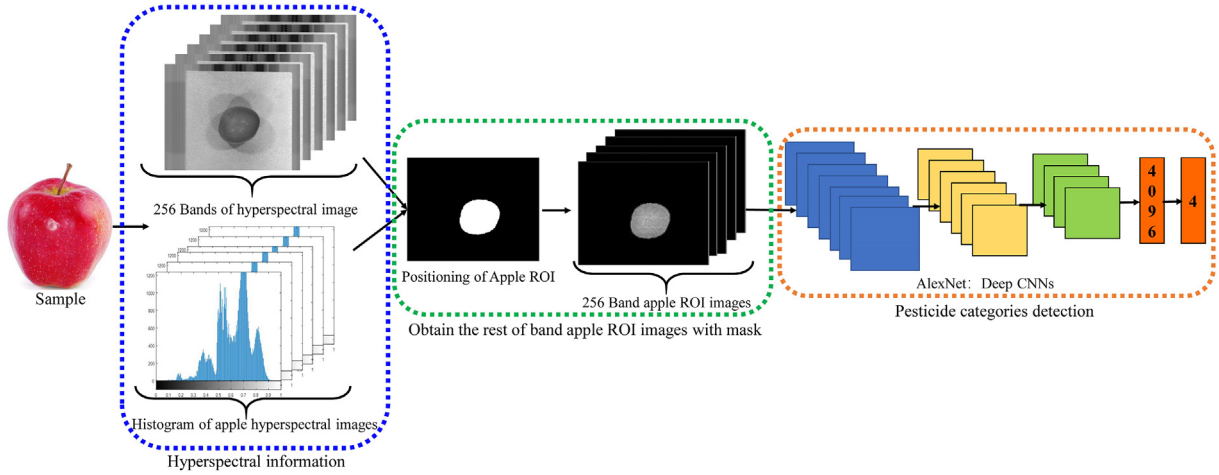

Fig. 2. Proposed algorithm flowchart.

area of the apple was fixed in the center of the image, meaning that the invalid image area could be eliminated by extracting the ROI information for the position of the apple.

2.2. Hyperspectral preprocessing of the apple image using machine vision technology

Fig. 2 shows the flow chart for the algorithm.

2.2.1. Positioning of the ROI for the apple

The Otsu segmentation algorithm uses an optimal threshold that is selected automatically to divide the original image into foreground and background (Kwong et al., 2018). Fig. 3a shows a hyperspectral image of an apple with a certain band, and Fig. 3b shows a hyperspectral gray histogram. It can be seen from Fig. 3 that the hyperspectral image of the apple is a multi-peak image in which the sub-peaks of each peak are different, that is, they are relatively independent. This multi-peak image is therefore considered to be a linear superposition of multiple single peaks. The Otsu segmentation algorithm can be used to process the hyperspectral images to obtain rough pixel regions for the apples, and the binary image obtained in this way is subjected to a morphological operation to eliminate non-ROI interference and segment the final ROI region for the apple. The obtained Otsu segmentation image shown in Fig. 4a is pixel-filled to give binary padding, as shown in Fig. 4b, and the pixel area value of each white pixel block is calculated separately. The other pixel areas that are smaller than a factor of 0.05 of the maximum region are filtered to obtain the image in Fig. 4c. The roundness ($0 \le R_N \le 1$) of each connected area is then calculated according to Eq. (1), and the connected area with the largest roundness value is the apple ROI area, as shown in Fig. 4d.

$$R_N = \frac{4\pi S}{C^2} \tag{1}$$

where S is the area of the pixel block in the connected domain, C is the perimeter of the pixel block in the connected domain, the units are pixels, and R_N represents the roundness of the pixel block in the connected domain.

2.2.2. Extraction of ROI for the apple

The obtained ROI position image is used as a mask $M(x, y)$ for extracting other bands, and the ROI of the remaining band is calculated according to Eq. (2).

$$f_{ROI}(x, y) = M(x, y)F(x, y) \tag{2}$$

where $F_{ROI}(x, y)$ is the ROI image of the extracted from the band, and $F(x, y)$ is the hyperspectral image of the remaining bands. As shown in Fig. 5, the ROI mask for the apple and the remaining band image undergo a mathematical operation to obtain the ROI for the apple of the remaining band, and this lays the foundation for the CNN to carry out feature extraction.

2.2.3. Construction of the CNN network

A CNN is a type of deep network used in the deep learning model. Compared with a traditional neural network model, a CNN has fewer

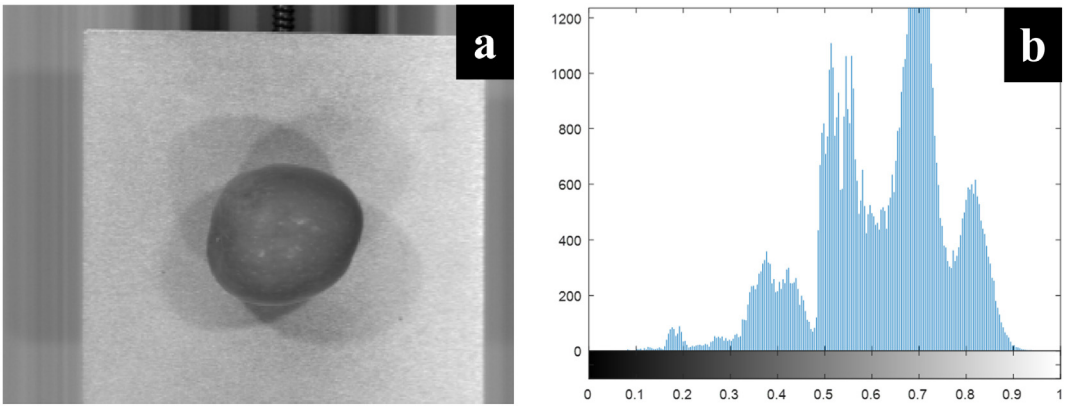

Fig. 3. Apple hyperspectral image and its Histogram. (a) Apple hyperspectral images (b) Histogram of apple hyperspectral images (the x-axis represents the frequency at which the pixel value appears, and the y-axis represents the number of pixel values).

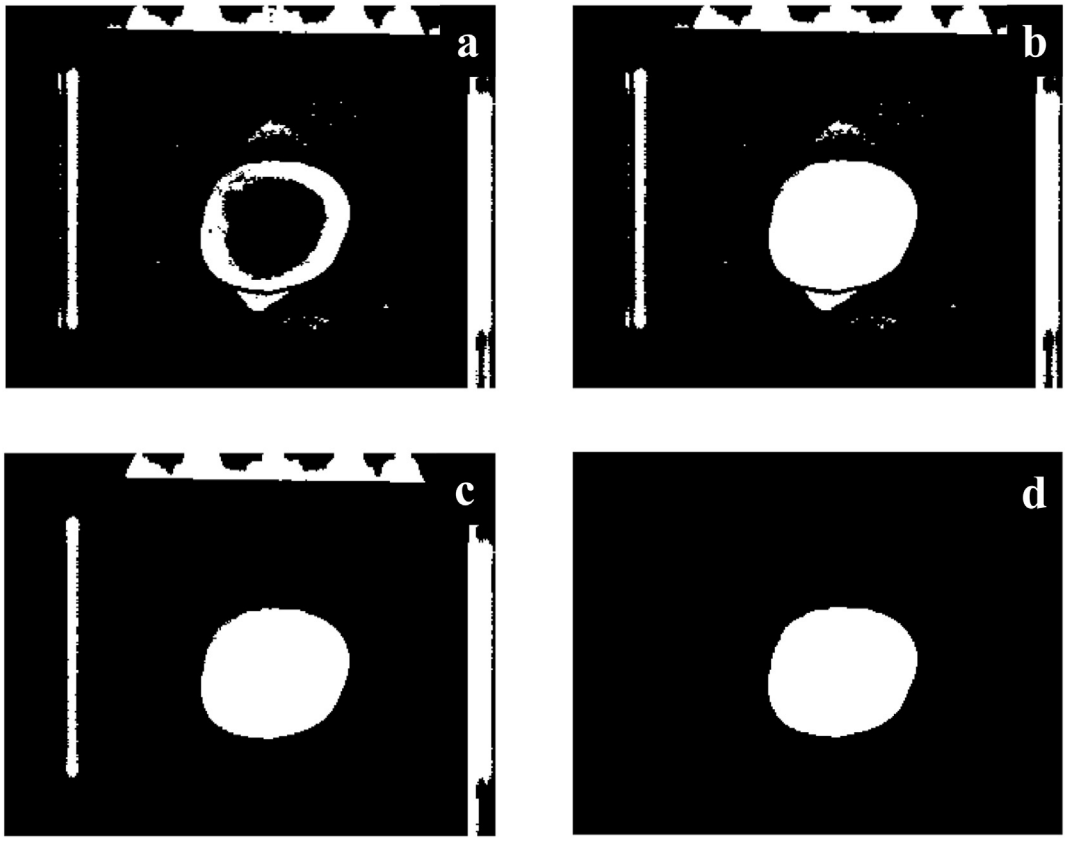

Fig. 4. Obtain binary images of apple's ROI area. (a) Otsu segmentation result. (b) Image filling. (c) Filtering smaller pixel blocks. (d) Extracting pixel blocks with the largest roundness.

parameters and stronger expressive power, and can automatically extract effective feature structures from complex spectral data (Lawrence et al., 1997). AlexNet is a CNN network with a relatively shallow network structure, and is capable of extracting rich features from images (Yuan and Zhang, 2016).

The hyperspectral data for each apple pesticide residue is used as a category or model. The detection of pesticide residues in apples requires matching and predicting unknown pesticide residue categories. The number of grades of apple pesticide residues in the sample is used as the number of matching categories or recognition patterns. A total of 18,432 spectral data images are included in the four types of samples. A CNN is required with a fast training time, a relatively shallow network structure, and efficient extraction of feature information from spectral data, and the AlexNet network architecture meets these conditions. Based on the above analysis of the hyperspectral data characteristics of apple pesticide residues, an AlexNet CNN framework that was suitable for the detection of apple pesticide residues was constructed.

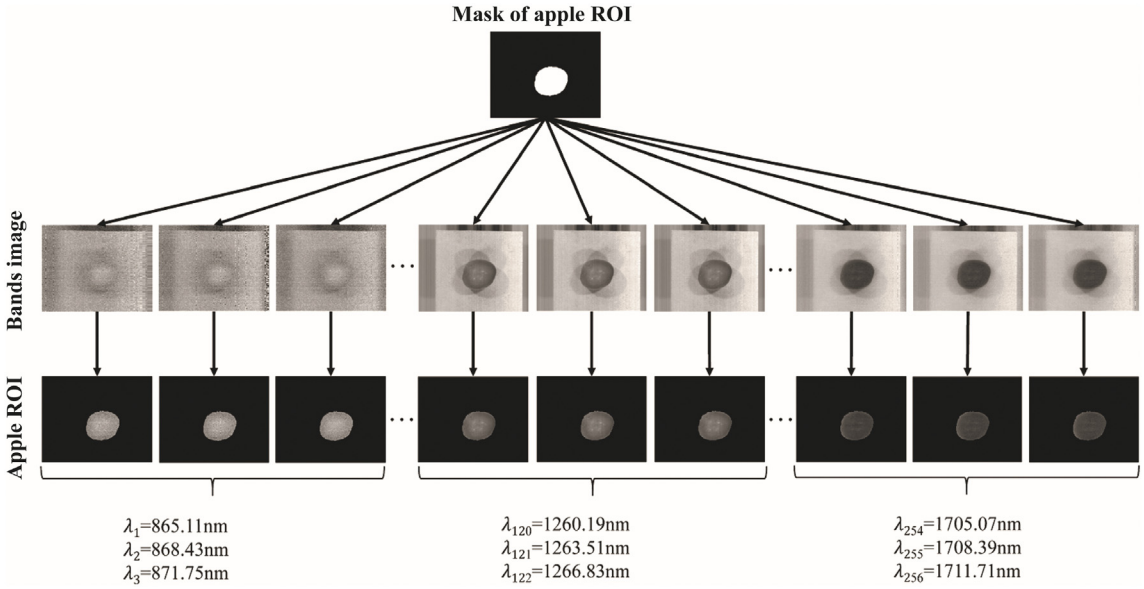

Fig. 5. Obtain the rest of band apple ROI images with mask.

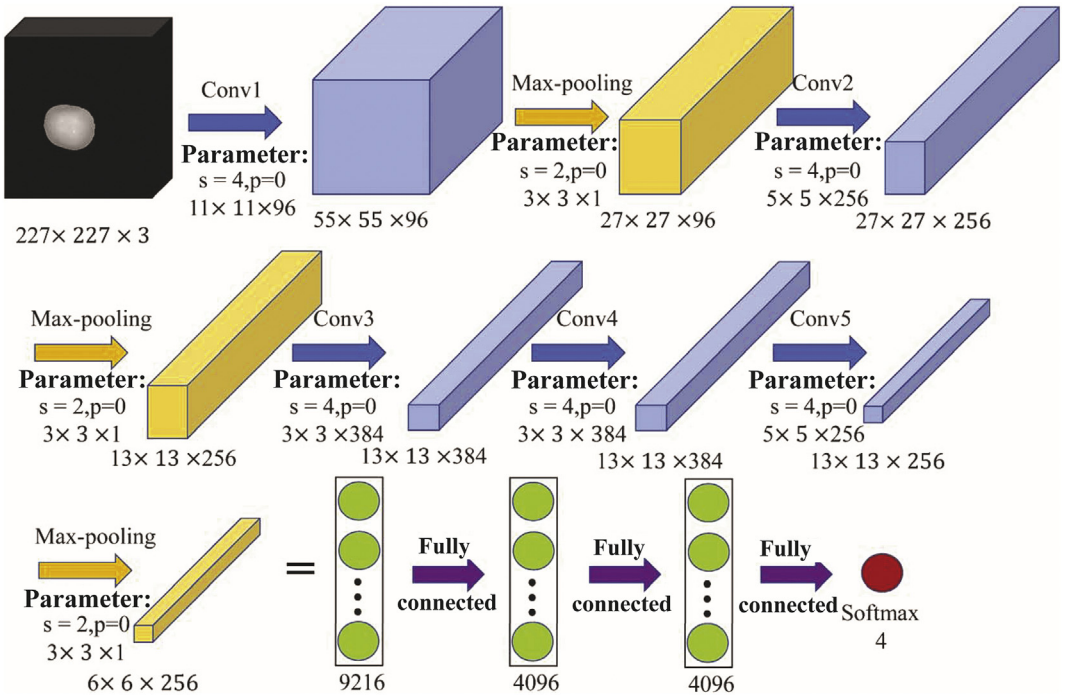

Fig. 6. CNNs network structure presented in this research.

2.3. Image classification method in traditional machine learning

The classification of hyperspectral data for the apple pesticide residues involved in this study is a typical image classification problem; based on hyperspectral data maps for different apple pesticide residue types, particular characteristics reflected by the same target object are divided into one type. In this study, in order to ensure that as many details as possible are input into the hyperspectral data map, the image size for the agricultural residue hyperspectral data was normalized to $227 \times 227 \times 3$ pixels.

Since no problems such as deformation of the position of the apple in the hyperspectral image are encountered, a framework of five convolutional layers and three fully connected layers was used in this work. In addition, a three-layer max-pooling layer was also adopted to improve the network's utilization rate of the feature information for the hyperspectral data images for the different types of apple pesticide residues. When pooling, the output matrix of the previous layer is maximized based on the superparameters of the pooled layer, and the pooled layer has no weight or offset value. I Information matching was realized using the Softmax function. In this study, there are four different apple pesticide residues, and Softmax therefore contains four perceptrons.

The biologically similar ReLu activation function was used as the activation function. Compared to a sigmoid function, it has three major advantages: (i) unilateral inhibition; (ii) a relatively wide threshold excitation boundary; and (iii) sparse activation (Glorot et al., 2012). Finally, the network structure of the CNN shown in Fig. 6 was selected for this research.

The blue arrow in Fig. 6 represents the convolution process, and the light blue color represents the output after convolution; the yellow arrow represents the maximum pooling process, and the lighter yellow indicates the output after maximum pooling; the purple arrow represents the process of fully connecting the extracted feature values. The light green color shows each feature extracted using the above network, and the red represents the Softmax classifier, which contains four perceptrons. The specific parameters used are shown in Table 1.

In order to further compare the advantages and disadvantages of the CNN for the AlexNet architecture with traditional image classification methods, we carry out a comparison of this approach with two common image classification methods, SVM (Hearst et al., 2002) and KNN (Cost and Salzberg, 1993). In this paper, the brightness feature was extracted from the hyperspectral data and used as the basis of image classification, before SVM and KNN classification were used to classify the apple pesticide residues in the data.

The SVM image classification method gives a hyperplane in the feature space for hyperspectral data samples of different apple pesticide residues. The brightness feature of the hyperspectral data images are classified by this hyperplane, i.e. this is a classification of hyperspectral images. The KNN image classification method can give the similarity between the brightness features in the high spectrum of the apple pesticide residues based on the distance metric, i.e. a brightness feature with high similarity indicates that the hyperspectral data image for the pesticide residue type is highly likely to be a certain species. The key parameters for the two algorithms used in comparative experiment are shown in Table 2.

3. Results and discussion

3.1. Classification results and analysis

The CNN was trained using a training set of 12,288 hyperspectral data map samples, and the minimum loss function and network parameters

Table 1
Parameters of each layer in the convolutional neural network.

Layer name	Size	Number	Stride	Padding
Conv1	11×11	96	4	0
Maxpooling1	3×3	1	2	0
Conv2	5×5	256	4	0
Maxpooling2	3×3	1	2	0
Conv3	3×3	384	4	0
Conv4	3×3	384	4	0
Conv5	5×5	256	4	0
Maxpooling3	3×3	1	2	0

Table 2
Values of key parameters for the SVM and KNN methods.

SVM		KNN	
Parameters	Values	Parameters	Values
Num. class	4	Num. class	4
Cost function	Square function	Cost function	Square function
Class design	One-to-many	Distance metric	Euclidean distance

Table 3
Detection rate and efficiency of CNN.

Net name	Detection rate/%		Elapsed time/s	
	Single image	Test set	Single image	Test set
CNN	95.35	99.09	0.0846	8.0691

were obtained using mini-batch gradient descent (MBGD) (Li et al., 2017). The initial parameters used in the CNN in this study are as follows: time decay: 0.0005; momentum parameter: 0.9; batch size: 32; one epoch: 384 iterations; number of epochs: 10. After the tenth training iteration, the network was verified using a sample set of 6144 hyperspectral data images. The results are shown in Table 3. As can be seen from the table, the CNN constructed here can detect the hyperspectral images of single apple pesticide residues and the hyperspectral test atlas of apple pesticide residues with accuracies of 90.55% and 99.11%, respectively. The average time required is also low enough to meet the requirements of real-time detection.

Of 6144 hyperspectral data images of apple pesticide residues in the testing set, 0.91% were detected incorrectly (56 images). Fig. 7 shows sample number 42 in category B (wavelength 1545.71 nm) and sample number 60 in category K (wavelength 1545.71 nm) for which detection errors occurred. The image details are lost after changing the size of the image and max-pooling, making it difficult for the constructed network to distinguish between similar images. Thus, when two hyperspectral images are in the same band and have similar appearances, the network will generate detection errors.

In order to further improve the accuracy of detection for hyperspectral images of apples with similar appearance in the same band, the number of specific features in the convolution kernel can be increased, i.e. the individual feature information of the apples in the hyperspectral images is increased to ensure that there are larger differences between similar apples in the same band.

3.2. Analysis of the characteristic diagram

Fig. 8 shows the corresponding feature image results for hyperspectral images of apples obtained by the convolution layer and the max-pooling layer in the CNN. Since the images are normalized before input, the numerical distribution interval of each feature image matrix obtained is [0, 1] (Vahadane et al., 2016; Garain et al., 2018; Zanjani et al., 2018).

By comparing the input image in Fig. 8 with the image obtained from the b-convolution layer, we can see that the 96 convolution kernels in the b-convolution layer extract image features such as the outline of the input image, bright and dark pixel areas, etc. Since the obtained image features have a smoothing effect, the input image can be considered as having been filtered 96 times through a convolution kernel, and each convolution operation can improve the anti-interference capability of the network. The c max-pooling layer is used to enlarge the image features obtained by the b convolution layer, the f omission layer includes three convolution layers and two max-pooling layers, and the g fully connected layer connects all the extracted image features. This operation can reduce the solution parameters and extract the main feature information from the image, which can give a better detection effect.

3.3. Comparison with image classification methods in traditional machine learning

The training and testing sets of the CNN were used as the training and testing sets for the SVM and KNN classification algorithms in the traditional image classification process, and the performance of these three algorithms was compared. Values for the accuracy and time costs of the hyperspectral image detection of pesticide residues in apples are shown in Table 4.

In the KNN and SVM classification algorithms, classification is based on information in the brightness feature of hyperspectral images. Due to the use of hyperspectral data images, the brightness information of images in the same band is very similar. The Euclidean distance (Mesquita et al., 2017), which is used to calculate the brightness feature information of each image, is also very close, so the correct rate for hyperspectral apple pesticide residue detection is as low as 43.75%, and the time consumption is 0.7645 s. Using its non-linear mapping characteristics, SVM divides the brightness feature space for the hyperspectral images into optimal hyperplanes and maximizes the classification boundary, and the classification detection accuracy of SVM is therefore higher than that of KNN. In summary, a CNN using the AlexNet framework has robust anti-interference ability, and the detection process has a low time cost; at the same time, it also has high robustness to the image brightness characteristics.

4. Conclusion

(1) In this study, a CNN based on AlexNet was constructed. Detection results for 6144 images of four kinds of hyperspectral apple pesticide residue showed that the average recognition rate for

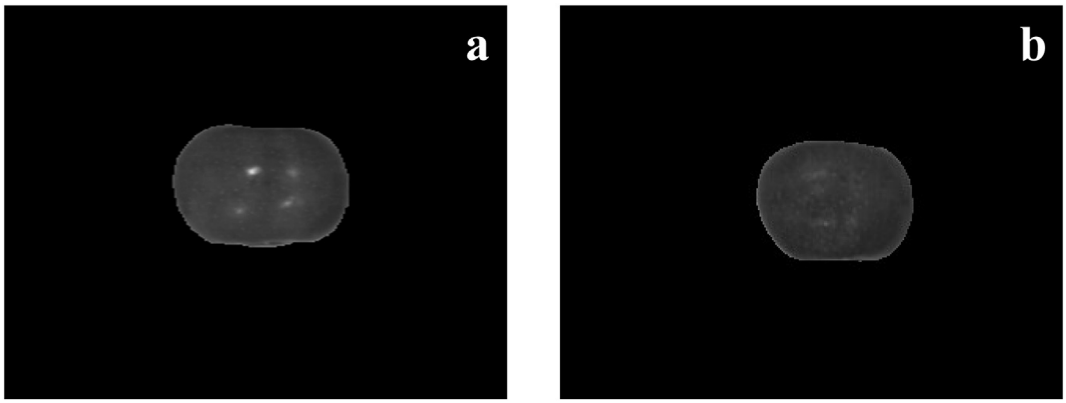

Fig. 7. Hyperspectral images of crisscross detection. (a) B concentration sample No. 42 (λ = 1545.71 nm). (b) K concentration sample No. 60 (λ = 1545.71 nm).

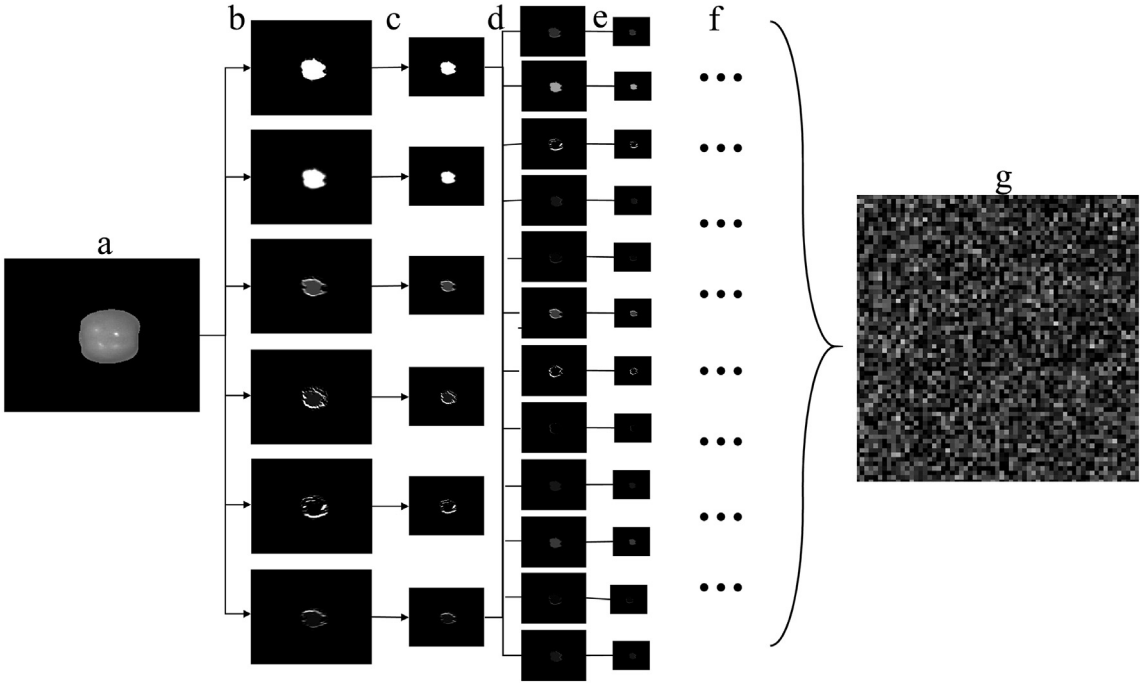

Fig. 8. Results in each layer (part) of CNNs. (a) Input layer. (b) Convolutions layer (part connection). (c) Max-pooling layer (d) Convolutions layer (part connection). (e) Max-pooling layer. (f) Omit layer. (g) Full connection layer.

single-band images was 95.35%, and the true positive detection rate for the test set was 99.09%. There was no overlap between the test samples and the training samples, and this shows that the network has strong generalizability.

(2) The Otsu segmentation algorithm was used to detect binary images containing the ROI for the apple in hyperspectral images. The roundness analysis of the binary image can obtain an effective mask for the ROI of the apple and eliminate the invalid region.

(3) Compared with the SVM and KNN methods, the CNN has the advantages of low time cost and high robustness. However, when two hyperspectral images are in the same band and have a similar appearance, the network is prone to detection errors. In future research, the number of specific feature parameters of the convolution kernel could be increased as the basis of network classification, in order to improve the feature extraction ability of the network for similar hyperspectral images of apples in the same band, and to further improve the accuracy of pesticide residue detection.

Acknowledgments

This work was supported by the National Natural Science Foundation of China (Grant No. 31501228) and the Yangling Demonstration Zone Science and Technology Plan Project (Grant No. 2016NY-31).

Compliance with ethical standards

This article does not involve any studies with human or animal subjects.

Table 4
Comparison of image classification methods and CNN.

Algorithm	Recognition rate/%	Time/s
KNN	43.75	0.7645
SVM	74.34	11.2301
CNNs	99.09	0.0846

Conflict of interest

Bo Jiang declares that he has no conflict of interest. Jinrong He declares that he has no conflict of interest. Hongfei Fu declares that he has no conflict of interest. Tong Li declares that he has no conflict of interest. Huaibo Song declares that he has no conflict of interest. Dongjian He declares that he has no conflict of interest. Yun Zhao declares that she has no conflict of interest.

Informed consent

Not applicable.

References

Cost, S., Salzberg, 1993. A weighted nearest neighbor algorithm for learning with symbolic features. Mach. Learn. 10 (1), 57–78.
Czernyszewicz, E., 2016. Long-term trends in production and consumption of apples in Poland, Europe and worldwide. Acta Sci. Pol. 15 (3), 95–104.
Garain, J., Kumar, R.K., Kumar, D., Kisku, D.R., 2018. Image specific cross cohort normalization for face pair matching. Proc. Comput. Sci. 132, 1060–1067.
Glorot, X., Bordes, A., Bengio, Y., 2012. Deep sparse rectifier neural networks. International Conference on Artificial Intelligence and Statistics, pp. 315–323.
Hearst, M.A., Dumais, S.T., Osuna, E., Platt, J., 2002. Support vector machines. IEEE Intell. Syst. 13 (4), 18–28.
Jia, Song, Lihua, Song, Yue, Chen, Jianhui, Zhang, Wu, Hao, 2017. The influence of cleaning methods on pesticide residue removal effect of fruits and vegetables. Food Res Dev 38 (20), 160–164.
Jiang, S., Sun, J., Xin, Z., Mao, H., Wu, X., 2016. Visualizing distribution of pesticide residues in mulberry leaves using NIR hyperspectral imaging. J. Food Process Eng. 40 (4).
Jiyun, Nie, Zhixia, Li, Chuande, Liu, Jinbao, Fang, Wang, Cheng, Guo, Yongze, Shaorong, Lei, Haifei, Li, Xu, Guofeng, 2014. Risk assessment of pesticide residues in apples. Sci. Agric. Sin. 47 (18), 3655–3667.
Kwong, S.T.W., Gao, H., Pun, C.M., 2018. An improved artificial bee colony algorithm with its application to metallographic image segmentation. IEEE Trans. Ind. Inf. 99, 1.
Lawrence, S., Giles, C.L., Tsoi, A.C., 1997. Face recognition: a convolutional neural-network approach. IEEE Trans. Neural Netw. 8 (1), 98–113.
Li, J., Li, X., Zhao, L., 2017. Hyperspectral unmixing via projected mini-batch gradient descent. IEEE International Geoscience and Remote Sensing Symposium, pp. 1133–1136.
Liang, Ke, Xie, Junping, 2017. Current status and breakthrough of rapid detection technology for pesticide residues in fruits and vegetables. China Food Saf. Mag. 31, 32–33.
Mesquita, D.P.P., Gomes, J.P.P., Junior, A.H.S., 2017. Euclidean distance estimation in incomplete datasets. Neurocomputing 248, 11–18.
Peng, Lei, Lv, Shaobo, Li, Ye, 2014. Multispectral fluorescence imaging technology for pesticide residues detection. Chin. J. Lumin. 35 (6), 748–753.

Vahadane, A., Peng, T., Sethi, A., 2016. Structure-preserving color normalization and sparse stain separation for histological images. IEEE Trans. Med. Imaging 35 (8), 1962–1971.
Wang, Z., Hu, M., Zhai, G., 2018. Application of deep learning architectures for accurate and rapid detection of internal mechanical damage of blueberry using hyperspectral transmittance data. Sensors 18 (4), 1126.
Wei, Zhou, 2017. Determination of organophosphorous pesticides in cider by GC-MS coupled with cloud point extraction. Sci. Technol. Food Ind. 23, 225–231.
Yande, Liu, Xie, Qinghua, Wang, Haiyang, Ma, Kuirong, 2017. Quantitative study on phosmet residues in navel oranges based on surface enhanced Raman spectra. Laser Technol. 41 (4), 545–548.
Yuan, Z.W., Zhang, J., 2016. Feature extraction and image retrieval based on AlexNet. Eighth International Conference on Digital Image (100330E).
Zanjani, F.G., Zinger, S., Bejnordi, B.E., Laak, 2018. Stain normalization of histopathology images using generative adversarial networks. IEEE International Symposium on Biomedical Imaging, pp. 573–577.
Zengfang, Li, Bingquan, Chu, Hailiang, Zhang, He, Yong, Xuemei, Liu, 2016. Study on nondestructive detecting gannan navel pesticide residue with hyperspectral imaging technology. Spectrosc. Spectr. Anal. 36 (12), 4034–4038.
Zhang, M., Li, C., 2018. Fully convolutional networks for blueberry bruising and calyx segmentation using hyperspectral transmittance imaging. 2018 ASABE Annual International Meeting. American Society of Agricultural and Biological Engineers, p. 1.
Zhu, Wenxiu, Wei, Zhuang, Jianzhong, Liu, Yunqi, Tang, 2017. Laser detection of apple pesticide residues. Sci. Technol. Inf. 15 (15), 116–117.